ANL/RE/CP--86313

CONF-950740--57

STRUCTURAL RESPONSE OF RECTILINEAR CONTAINMENT TO OVERPRESSURIZATION

P. A. Pfeiffer and R. F. Kulak
Reactor Engineering Division
Argonne National Laboratory
Argonne, Illinois

ABSTRACT

Containment structures for nuclear reactors are the final barrier between released radionuclides and the public. Containment structures are constructed from steel, reinforced concrete, or prestressed concrete. U.S. nuclear reactor containment geometries tend to be cylindrical with elliptical or hemispherical heads. The older Soviet designed reactors do not use a containment building to mitigate the effects of accidents. Instead, they employ a sealed set of rectilinear, interconnected compartments, collectively called the accident localization system (ALS), to reduce the release of radionuclides to the atmosphere during accidents.

The purpose of this paper is to present a methodology that can be used to find the structural capacity of reinforced concrete structures. The method is applicable to both cylindrical and rectilinear geometries. As an illustrative example, the methodology is applied to a generic VVER-440/V213 design.

INTRODUCTION

To assure the structural integrity of critical reactor structures, such as containments/confinements, it is necessary to simulate their structural response to design and beyond-design-basis loadings. Because of the complexity of the structures and the highly nonlinear physics that occurs, the use of three-dimensional numerical methods is necessary. Rectilinear containment structures, in particular, require three-dimensional analysis. The Reactor Analysis Division of Argonne National Laboratory has developed software, NEPTUNE (Kulak, et al., 1988), specifically designed for the three-dimensional analysis of containments. This paper describes the methodology used to analyze reinforced concrete structures to overpressure. The method is then applied to the analysis of a generic VVER-440/V213 confinement structure. The capabilities presented here would also be applicable to U.S. type containment.

The methodology presented here was used to find the ultimate structural capacity of the confinement structures and to identify probable failure sites. Complex, three-dimensional, finite-element models were developed to represent the main structural components of the confinement. The NEPTUNE (Kulak, et al., 1988) three-dimensional, nonlinear finite element code was used to simulate the response of the confinement. The interior boundary of the localization system was incrementally pressurized in the calculations until the prediction of gross failure.

METHODOLOGY

This section describes the methodology used to simulate the response of reinforced concrete structures to overpressure. The first subsection describes the reinforced concrete plate element and the second subsection describes the constitutive model and failure criteria.

Reinforced Concrete Element

The analysis of large, complex RC structures requires the use of numerically accurate and efficient finite elements. These elements must be capable of handling both static and dynamic loadings. An element that has most of the desired features was developed by Belytschko, et al. (1984). The element was further developed by Kulak and Fiala (1988) by incorporating the features to represent concrete, and reinforcing steel. Subsequently, additional failure criteria were added, and now the element can model concrete cracking, rebar failure, and gross transverse failure.

The element is a four-node quadrilateral plate element (Fig. 1) that uses a one-point integration scheme along with hourglass control. The element uses corotational coordinates and thus eliminates the need for Jaumann rate corrective terms. The corotational coordinate system $(\hat{x},\hat{y},\hat{z})$ is defined in Fig. 1. The

DISCLAIMER

Portions of this document may be illegible in electronic image products. Images are produced from the best available original document.

notation x_{IJ} is used to indicate the difference between coordinates at two nodes (e.g., $x_{IJ} = x_I - x$). The velocity strain, d_{ij} is given by

$$\begin{aligned}
\hat{d}_{xx} &= B_{1I}\hat{v}_{xI} + \hat{z}B_{1I}\hat{\theta}_{yI},\\
\hat{d}_{yy} &= B_{2I}\hat{v}_{yI} - \hat{z}B_{2I}\hat{\theta}_{xI},\\
2\hat{d}_{xy} &= B_{2I}\hat{v}_{xI} + B_{1I}\hat{v}_{yI} + \hat{z}\left(B_{2I}\hat{\theta}_{yI} - B_{1I}\hat{\theta}_{xI}\right),
\end{aligned} \tag{1}$$

where $\hat{v}_{iI}$ is the velocity, $\hat{\theta}$ is the angular velocity at node I in the ith local coordinate direction, and $\hat{z}$ is the depth dimension. The B_{iI} are given by

$$B_{iI} = \frac{1}{2A}\begin{bmatrix} \hat{y}_{24} & \hat{y}_{31} & \hat{y}_{42} & \hat{y}_{13} \end{bmatrix} \quad \text{, (for i=1)}$$
$$B_{iI} = \frac{1}{2A}\begin{bmatrix} \hat{x}_{42} & \hat{x}_{13} & \hat{x}_{24} & \hat{x}_{31} \end{bmatrix} \quad \text{, (for i=2)} \tag{2}$$

The nodal internal forces are given by

$$\begin{aligned}
\hat{f}_{xI} &= A\left(B_{1I}\hat{f}_x + B_{2I}\hat{f}_{xy}\right),\\
\hat{f}_{yI} &= A\left(B_{2I}\hat{f}_y + B_{1I}\hat{f}_{xy}\right),\\
\hat{f}_{zI} &= A\bar{\kappa}\left(B_{1I}\hat{f}_{xz} + B_{2I}\hat{f}_{xy}\right),\\
\hat{m}_{xI} &= A\left[B_{2I}\hat{m}_y + B_{1I}\hat{m}_{xy} - 0.25\bar{\kappa}\hat{f}_{yz}\right],\\
\hat{m}_{yI} &= A\left[-B_{1I}\hat{m}_x - B_{2I}\hat{m}_{xy} + 0.25\bar{\kappa}\hat{f}_{xz}\right],\\
\hat{m}_{zI} &= 0,
\end{aligned} \tag{3}$$

where $\bar{\kappa}$ is the shear factor, and A is the planer area of the element.

The left portion of Fig. 2 shows a section through the thickness of a concrete wall/slab that has layers of arbitrarily oriented rebars embedded in the wall. The right portion of the figure shows that each discrete layer of individual rebars are modeled as distinct layers in the computer code. The contribution to the internal forces and moments from the concrete are given by

$$\hat{f}^{con}_{\alpha\beta} = \int \hat{\sigma}^{con}_{\alpha\beta}\, d\hat{z}, \qquad \hat{m}^{con}_{\alpha\beta} = -\int \hat{z}\hat{\sigma}^{con}_{\alpha\beta}\, d\hat{z}. \tag{4}$$

where $\sigma^{con}_{\alpha\beta}$ is the concrete stress. Similarly, for the rebars the contribution to the internal forces and moments are given by

$$\hat{f}^{rb}_{\alpha\beta} = \sum_{I=1}^{L} \frac{A_\ell}{p^\ell}\hat{\sigma}^\ell_{\alpha\beta}$$

and

$$\hat{m}^{rb}_{\alpha\beta} = -\sum_{\ell=1}^{L} \hat{z}^\ell \frac{A^\ell}{p^\ell}\hat{\sigma}^\ell_{\alpha\beta}, \tag{5}$$

where $\sigma^\ell_{\alpha\beta}$ is the rebar stress for a smeared layer ℓ, A^ℓ is the area of the layer, p^ℓ is the pitch of the rebars in the layer, and L is the number of rebar layers. Finally, the contributions of the liner, which is treated as a membrane, to the internal forces and moments are given by

$$\hat{f}^{\ell r}_{\alpha\beta} = \hat{\sigma}^{\ell r}_{\alpha\beta}h, \qquad \hat{m}^{\ell r}_{\alpha\beta} = -\hat{z}^{\ell r}\hat{\sigma}^{\ell r}_{\alpha\beta}h, \tag{6}$$

where h is the thickness of the liner.

The element's internal forces and moments are equal to the sum of the contributions from the responses of the concrete, rebars, and linear, that is,

$$\begin{aligned}
\hat{f}_{\alpha\beta} &= \hat{f}^{con}_{\alpha\beta} + \hat{f}^{rb}_{\alpha\beta} + \hat{f}^{\ell r}_{\alpha\beta},\\
\hat{m}_{\alpha\beta} &= \hat{m}^{con}_{\alpha\beta} + m^{rb}_{\alpha\beta} + \hat{m}^{\ell r}_{\alpha\beta}.
\end{aligned} \tag{7}$$

Concrete Constitutive Model

A typical uniaxial compression-tension behavior of concrete is shown in Fig. 3. As seen in the figure, concrete has different strength limits in tension and compression and also exhibits nonlinearity even under low stress and strain values. The figure also shows that two different portions exist in the overall response, which are the strain-hardening and the strain-softening parts. An accurate analysis should take account of the above properties.

The concrete failure model utilized is the Hsieh-Ting-Chen (H-T-C) four-parameter model. The model described by Hsieh, et al. (1979) uses the following four-parameter criterion involving the stress invariants I_1, J_2 and the maximum principal stress σ_1:

$$f\left(I_1, J_2, \sigma_1\right) = a\frac{J_2}{f'^2_c} + b\frac{\sqrt{J_2}}{f'_c} + c\frac{\sigma_1}{f'_c} + d\frac{I_1}{f'_c} - 1 = 0 \tag{8}$$

which consists of a combination of the general octahedral $\tau_{oct} = f(\sigma_{oct})$ and Rankine's maximum-principal-tensile-stress criterion. In particular, it reduces to the Drucker-Prager criterion for a = c = 0, to the von Mises criterion for a = c = d = 0, and to the Rankine criterion for a = b = d = 0, $c = f'_c/f'_1$.

To evaluate the four parameters a, b, c, and d, it should be realized that not all failure states can be determined experimentally with the same accuracy. The parameters are determined so that they represent the following four failure states exactly:

1. Uniaxial compressive strength f'_c
2. Uniaxial tensile strength $f'_t = 0.1\ f'_c$
3. Equal biaxial compressive strength $f'_{bc} = 1.15\ f'_c$
4. Combined triaxial compression, $f'_{pc} = 0.8\ f'_c$

   $\left(f'_{cc} > f'_{pc}\right)$ $\qquad f'_{cc} = 4.2\ f'_c$

With Eq. (8) the strength capacity of the concrete in a multiaxial stress space can be characterized by the H-T-C four parameter failure surface. A von Mises type loading function is used to determine the elastic-plastic response. If the von Mises function is used alone, the same behavior is implied in both tensile and compressive regions which is not true for concrete. Therefore, the von Mises function is used in conjunction with the H-T-C failure criterion which would produce different tensile and compressive responses. The concept of the approach is schematically shown in the biaxial principle stress space in Fig. 4. The concrete response after failure is simulated using the element size independent cracking criterion established by Bazant and Oh (1983). In the uniaxial stress-strain relationship, a linear reduction of strength is specified from the ultimate stress down to zero.

Additionally, the transverse shear failure of a reinforced concrete slab is also considered by an empirical formula. These type of failure occur in the locations of junctures and corners, such as the wall and floor interfaces, wall and basemat junctures, etc. Aoyagi and Yamada (1979) have determined an estimate of the ultimate strength in shear for the reinforced concrete sections based on experimental data. The shear failure equation is based on the following factors: transverse yield strength at the reinforcement, the normal stress acting in the shear plane, and the compressive strength of the concrete. The equation for the ultimate normal shear stress, τ_u, is given as

$$\tau_u = \left\{0.05\left(pf_y - \sigma_v\right) + 0.5\right\}\sqrt{f'_c}$$
$$0.5 \le \tau_u \le 4.5\sqrt{f'_c} \qquad (9)$$

where τ_u is the shear stress (kg/cm^2), σ_v is the normal stress (kg/cm^2, f_y is the yield strength of reinforcement (kg/cm^2), p is the reinforcement ratio, and f'_c is the compressive strength of concrete (kg/cm^2). Note that in Eq. (9) τ_u is bounded by a minimum value of $0.5\sqrt{f'_c}$ and a maximum value of $4.5\sqrt{f'_c}$.

EXAMPLE

The older Soviet designed VVER-440 reactors do not use a containment building to mitigate the effects of accidents. Instead, these VVER-440 (Kulak, et al., 1989) units employ a sealed set of interconnected compartments, collectively called the accident localization system (ALS), to reduce the release of radionuclides to the atmosphere during accidents. The compartments are rectilinear rooms, in contrast to the cylindrical or spherical shapes used in other designs. This system is a confinement system designed to keep leakage less than about 15 volume %/day at 0.25 MPa (absolute). The use of an advanced pressure suppression system causes the confinements internal pressure to drop to atmospheric or subatmospheric in a relatively short time. Descriptions of the VVER accident localization structures may be found in the report DOE NE-0084 (1989), Overall Plant Design Descriptions VVER Water-Cooled, Water-Moderated Energy Reactor. The confinement system consists of two interconnected main structures: the reactor building and the bubbler-condenser tower. The reactor building contains the reactor pumps, steam generators, pressurizer, accumulators, and associated piping. The bubbler-condenser tower, which is divided into two main sections, contains racks of bubbler-condenser trays and four air locks. The design basis accident is a large break LOCA (Sienicki, et al., 1989).

Figure 5 depicts an outside view of a typical VVER-440 reactor. The left side structure is the reactor building and the right side structure is the bubbler-condenser tower. A corridor is provided to allow the resulting accident overpressure to pass from the reactor building to the bubbler tower. The reference direction of Fig. 5 has north coming out of the page, thus east is on the left side of the figure and west is on the right side of the figure.

Reactor Building

The reactor building (left side of Fig. 5) houses the reactor, pumps, steam generators, pressurizer, accumulators, and piping. These components are located throughout the building in separate interconnected reinforced concrete compartments. Within the reactor building there is a sealed boundary called the "hermetic" boundary. The purpose of this boundary is to confine radioactive release within the space defined by it. For the most part, this boundary consists of 6 mm steel plates that are either attached to or embedded within the concrete walls, floors, and ceilings. The left side of Fig. 6 shows how the reactor building is constructed by compartments. The lower floor at 6m is the steam generator floor and the circular floor at 10m is the pump room floor. The operating floor at 18.9m is the next major floor. The operating floor supports three corner structures that rise to about 25m and contain accumulators, etc. The structure around the reactor shaft is also supported by the operating floor and is built up to the 21m level.

The reactor is positioned in the reinforced concrete cylindrical reactor shaft. The reactor shaft starts at the -6.50 m level and extends to the 21.0 m level. The bottom of the shaft is sealed by a thick basemat. The top of the shaft is sealed by a steel cap, which is part of the hermetic boundary. The somewhat circular pump room surrounds the upper reactor shaft from the 10 m level up to the operating floor at the 18.9 m level. The pump room is supported by 14 reinforced concrete columns at its outer periphery. The columns are anchored to the steam generator floor. The pump room is inside the steam generator room, which is a box-like reinforced concrete structure with the assumed following outside dimensions: 48 m (157 ft) long, 39 m (128 ft) wide, and 16 m (53 ft) high. The steam generator room floor is at the 6.0 level. The operating floor is the ceiling of the steam generator compartment. The main structural walls of the steam generator compartment are part of the hermetic

boundary. The front wall (west wall) has two openings that lead into the corridor between the steam generator room and the bubbler-condenser tower. The modeling assumes that a 5.5 m (18 ft) wide by 6.9 m (22.6 ft) high opening in the wall provides a passageway to the bubbler-condenser tower. All walls and floors of the reactor building were assumed to be 1.5 m (4.9 ft) thick for this study. The wall thickness will vary throughout the reactor building for the real structure. However, diagonal reinforced concrete walls were assumed to be 0.75 m (2.5 ft) thick, and are located in the corners of the steam generator room. These walls reduce the ceiling span.

Bubbler-Condenser Tower

The other main confinement structure (right side of Fig. 5) is the bubbler-condenser tower with assumed dimensions 40 m (131 ft) wide, 32 m (105 ft) deep, and 40 m (131 ft) high. The bubbler-condenser tower, which is divided into two main sections (right side of Fig. 6), contains racks of bubbler-condenser trays and four air locks. The racks of bubbler-condenser trays are on left side of the bubbler tower and the four air locks are on the right as shown in Fig. 6. The outside walls and the roof are made from reinforced concrete. The hermetic boundary consists of a 6 mm thick steel liner that covers the inside of the walls and roof. A vertical interior wall divides the structure into two parts. The eastern part contains 12 levels of bubbler-condenser trays that are supported on 256 steel I-beams. The I-beams are securely anchored to the east outer wall and the central interior wall. The east wall has openings at the 6.0 m level to the corridor from the steam generator compartment. The western part is divided into four airlocks by reinforced concrete floors. There are several rooms located beneath the bubbler-condenser tower 6.0 m level floor, which is outside the hermetic boundary. For this structure, all walls and floors were assumed to be 1.5 m thick. The slab thicknesses of the real bubbler-condenser tower varied.

Reinforcement

The ALS exterior walls, floors and ceilings are assumed to be 1.5 m (4.9 ft) thick and contain orthogonal layers of reinforcement near their inside and outside faces. The ALS is elevated above grade level, supported by walls underlying the floor of the steam generator room.

The steel reinforcement in the ALS is assumed to be constructed from two orthogonal layers of reinforcement located near each surface of the walls, floors, and ceiling. The diameters of the reinforcement were assumed to be 40 mm (1.57 in.). The cover distance was assumed to be 5.0 cm (2.0 in.), and the pitch was taken as 20.0 cm (7.9 in.). The reactor shaft was assumed to have additional reinforcement layers.

Material Properties

The concrete used to construct the localization compartment is taken to be design brand M-400 (Baikov and Sigalov, 1981), assumed to have a compressive strength of 400 kg of force per square centimeter (5,689 lbs/in.^{2}). The yield strength is taken to be 200 kg of force per square centimeter (2,845 lbs/in.^{2}), and the ultimate strain 0.3%. Young's modulus is taken equal to 302 $\times$ 10^3 kg of force per square centimeter (4.3 $\times$ 10^6 lbs/in.^{2}) and Poisson's ratio 0.2.

The reinforcing steel in the localization compartment is assumed to be class A-III (Soviet designation) deformed bars (Baikov and Sigalov, 1981). The modulus of elasticity of the bars is taken to be 200 GPa (29 $\times$ 10^6 lbs/in.^{2}), the yield point 400 GPa (58 $\times$ 10^3 lbs/in.^{2}), the ultimate strength 600 GPa (87 $\times$ 10^3 lbs/in.^{2}), and the ultimate strain 19%. Since the reinforcing in spliced during construction, a 5% ultimate strain is assumed.

The inside surfaces of the walls of the ALS are assumed to be lined with 6 mm (0.24 in.) thick low carbon steel assumed to have properties similar to the Soviet carbon steel designated as 22K (Antikagn, 1986). The following material properties are assumed: Young's modulus of 207 GPa (30 $\times$ 10^6 lbs/in.^{2}), Poisson's ratio of 0.3, yield stress of 265 GPa (38 $\times$ 10^3 lbs/in.^{2}), ultimate strength equal to 431 GPa (62 $\times$ 10^3 lbs/in.^{2}), and an ultimate strain of 15.5%.

Three-Dimensional Structural Models

A complex finite element model of the localization compartments of a generic VVER-440 and the underlying supporting structures has been developed. The finite element model of the reactor building, shown in Fig. 7, includes the steam generator room, corner walls, pump room , cable corridor reactor shaft, refueling and storage ponds and the supporting walls. A slice through the model is shown in Fig. 8 and indicates the level of modelling. The total number of nodes was 3302 with 3519 quadrilateral elements and 26 beam elements. Note that the quadrilateral elements are used to represent the walls and floors and the beam elements (solid lines in Fig. 8) are used to represent the supporting columns. The columns span between the steam generator floor and pump room floor and also help support the steam generator floor.

Figure 9 shows the finite element model of the bubbler-condenser tower and the connecting corridor to the reactor building. The model includes representations of the four air locks, the condenser room, the supporting beams of the condenser trays, the corridor and the underlying support walls. In Fig. 10 the slice through shows how the beams span between the interior wall and the east wall of the bubbler tower. The model assumes that the beams are fixed on each end. The total number of nodes was 2696 with 2829 quadrilateral elements for reinforced concrete and 228 beam elements for the support of the condenser trays.

Results

The structural response of the ALS subjected to internal pressurization was obtained by the NEPTUNE code (Kulak and Fiala, 1988). In the reactor building incremental load steps of 0.04 MPa were applied. The bubbler-condenser tower had load steps of 0.02 MPa applied.

The maximum calculated displacement in the reactor building is towards the upper center of the south wall. The calculated displacement is given in Fig. 11. A magnified deformed plot of the model is given in Fig. 12, note the large outward displacement of the south wall. The displacement appears to be

linear up to 0.4 MPa overpressure. Nonlinear response is evident up to 1.0 MPa. At 1.0 MPa the reinforcement in the south wall reaches the assumed failure strain of 5%. Cracking of the concrete first occurs at 0.20 MPa in the south wall. As the pressure increases, more of the loading is taken by the reinforcement until the failure strain is reached in the bars.

The maximum calculated displacement in the bubbler - condenser tower is located in the roof at the center span toward the west wall. The calculated displacement is given in Fig. 13. A magnified deformed plot of the model is given in Fig. 14, note the large outward displacement of the roof. The displacement appears to be linear up to 0.4 MPa overpressure. Nonlinear response is evident up to 0.58 MPa. At 0.58 MPa the reinforcement in the roof reaches the assumed failure strain of 5%. Cracking of the concrete first occurs at 0.20 MPa in the roof. As the pressure increases, more of the loading is taken by the reinforcement until the failure strain is reached in the bars.

The NEPTUNE code is based on an explicit integration which is optimal for transient type problems. However, with a high mass proportional damping, quasi static problems can be solved. At each load step, equilibrium is obtained by satisfying both a force norm and a displacement norm. The force norm is based on a global balance of internal and external forces. The displacement norm is based on the change in displacement from one iteration to the next. Generally the force norm is set to 2% error between external and internal forces, and the displacement change is set to 0.1%. Figure 15 indicates the amount of iterations required for both models. The initial elastic response requires about 200-250 iterations. As the simulation progresses the iterations tend to reduce during the increase in loading, or at least stabilize. As the problem becomes more nonlinear, due to material behavior and large displacements the amount of iteration increases until failure is reached.

The other failure mode to consider is the shear failure in the locations of junctures and corners. Aoyagi and Yamada (1979) have determined an estimation of the ultimate strength in shear for reinforced concrete sections as described before. During the simulation in both models, the ultimate shear strength criterion was monitored. Shear failure will occur at 0.60 MPa overpressure in the reactor building model. The resulting crack pattern on the outside surface is depicted in Figs. 16a and 16b. The failure location is at the juncture of the south wall and the operating floor. Shear failure will occur at 0.54 MPa in the bubbler-condenser tower. The resulting crack pattern on the outside surface is shown in Figs. 17a and 17b. The failure location is at the juncture of the roof and the west wall.

The resulting crack patterns based on the overpressures for reinforcement failure are given in Figs. 18 to 21. Figures 18a and 18b depict the inside and outside surface cracks in the reactor building for the east and west walls at 1.0 MPa. Figures 19a and 19b show the inside and outside surface cracks in the reactor building for the west and south walls. Figures 20a and 20b depict the inside and outside surface cracks in the bubbler-condenser tower for the west and south walls at 0.58 MPa overpressure. Figures 21a and 21b indicate the inside and outside surface cracks for the east and north walls.

CONCLUSIONS

A methodology was described for the structural response of reinforced concrete structures to overpressure. A description of the reinforced concrete plate element was given, and the associated constitutive model and failure criteria were presented.

An example problem was described and solved for structural response and failure. The example was an analysis of the accident localization system (ALS) of a generic VVER-440 Soviet reactor.

The developed methodology has been shown to be capable of simulating the response of a rectilinear, reinforced concrete containment structure up to failure. The program can model concrete cracking, rebar tensile failure, and gross transverse failure of sections. It is applicable to general three-dimensional containment/confinement structures.

ACKNOWLEDGMENTS

Work performed under the auspices of the U.S. Department of Energy, Technology Support Programs, under Contract W-31-109-Eng-38.

REFERENCES

Antikagn, P. A., 1986, "Steels for Vessels Operating Under Pressure," NIIekonomika, Moscow (in Russian).

Aoyagi, Y., and Yamada, K., 1979, "An Experimental Approach to the Design of Network Reinforcement Against In-Plane Shear in Reinforced Concrete Containments," *Proceedings of Structural Mechanics in Reactor Technology,* Vol. J 4/7, pp. 1-10.

Baikov, V., and Sigalov, E., 1981, "Reinforced Concrete Structures: Reinforced Concrete Strength and Members," MIR Publishers, Moscow.

Bazant, Z. P., and Oh, B. H., 1983, "Crack Band Theory for Fracture of Concrete," *Material Struct.*, RELEM, Paris, France, Vol. 16, pp. 155-177.

Belytschko, T., Lin, J. I., and Tsay, C., 1984, "Explicit Algorithms for the Nonlinear Dynamics of Shells," *Computer Methods in Applied Mechanics and Engineering,* Vol. 42, pp. 225-251.

DOE-0084, Revision 2, 1989, "Overall Plant Design Descriptions VVER Water-Cooled, Water-Moderated Energy Reactor," U.S. Department of Energy, Washington, DC.

Hsieh, S. S., Ting, E. C., and Chen, W. F., 1979, "An Elastic-Fracture Model for Concrete," *Proceedings, 3rd Engineering Mechanics Division Specialists Conference, ASCE,* Austin, TX, pp. 437-440.

Kulak, R. F., and Fiala, C., 1988, "NEPTUNE: A System of Finite Element Programs for Three-Dimensional Nonlinear Analysis, *Nuclear Engineering and Design,* Vol. 106, No. 1, pp. 47-68.

Kulak, R. F., Fiala, C., and Sienicki, J. J., 1989, "Response of Soviet VVER-440 Accident Localization System to Overpressurization," *Proceedings of Structural Mechanics in Reactor Technology* , Vol. J, pp. 331-336.

Sienicki, J. J., and Horak, W. C., 1989, "Pressure Loadings of Soviet Designed VVER Reactor Release Mitigation Structures from Large-Break LOCAs," *Proceedings, Structural Mechanics in Reactor Technology*, Vol. J, pp. 319-324.

DISCLAIMER

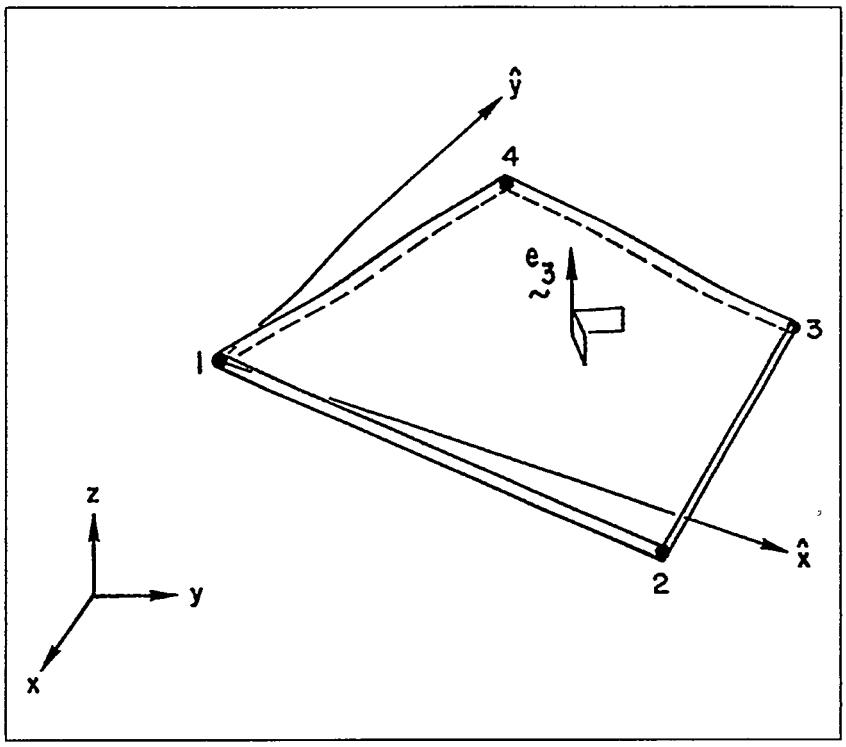

FIG. 1. QUADRILATERAL PLATE ELEMENT

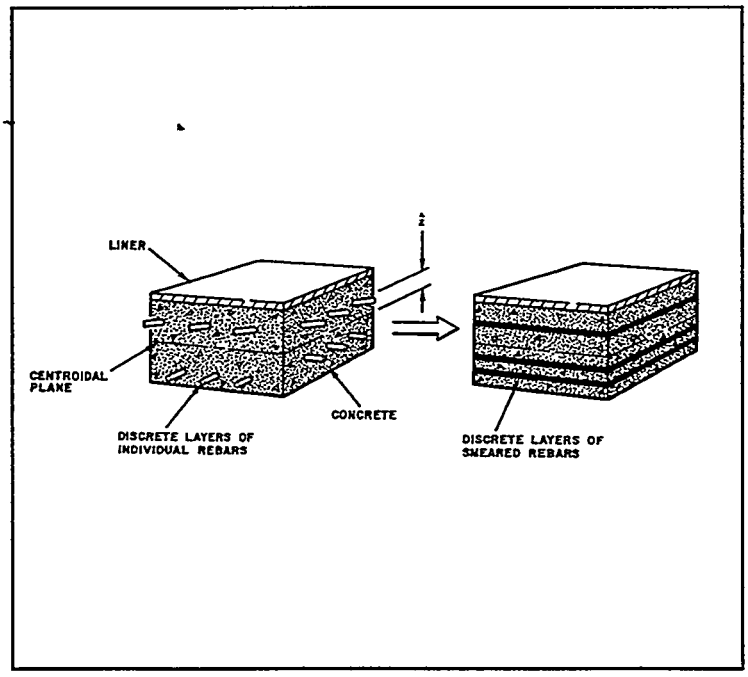

FIG. 2. REINFORCED CONCRETE ELEMENT MODEL

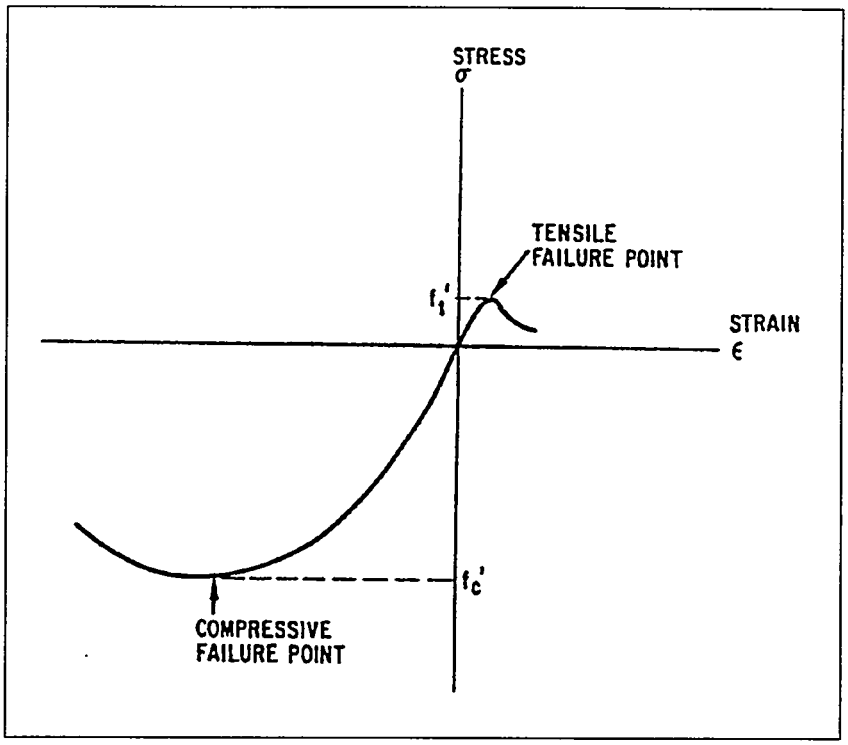

FIG. 3. COMPRESSION-TENSION BEHAVIOR OF CONCRETE

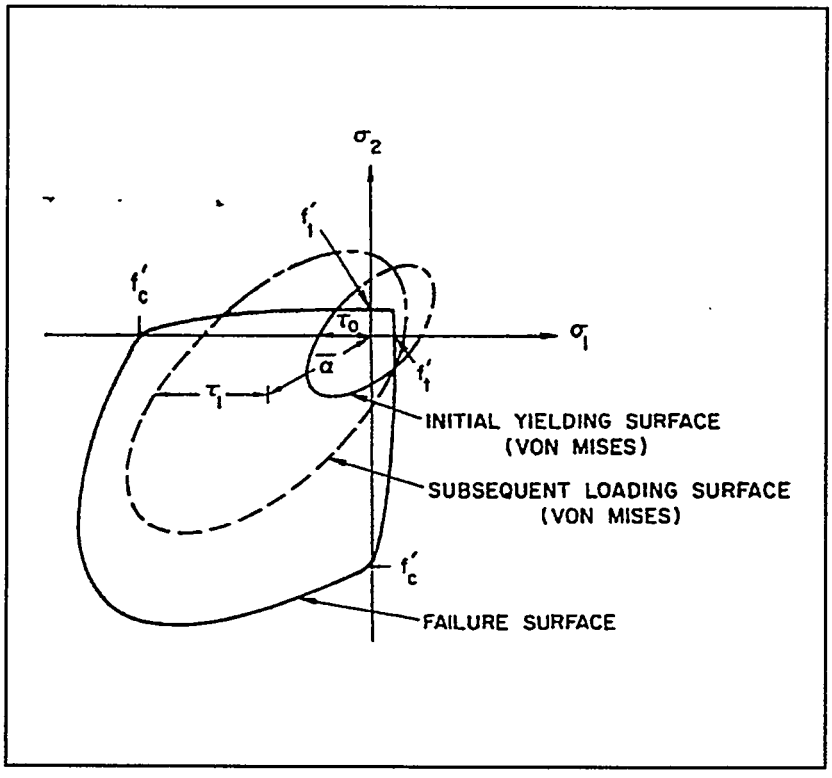

FIG. 4. SCHEMATIC REPRESENTATION OF THE VON MISES LOADING FUNCTION WITH THE FAILURE SURFACE

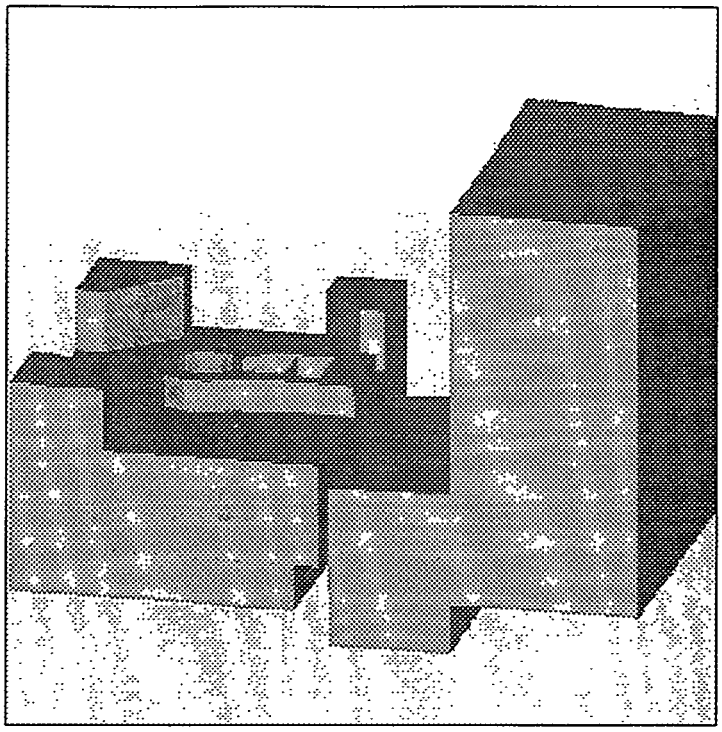

FIG. 5. OUTSIDE VIEW OF THE REACTOR BUILDING (LEFT) AND BUBBLER TOWER (RIGHT)

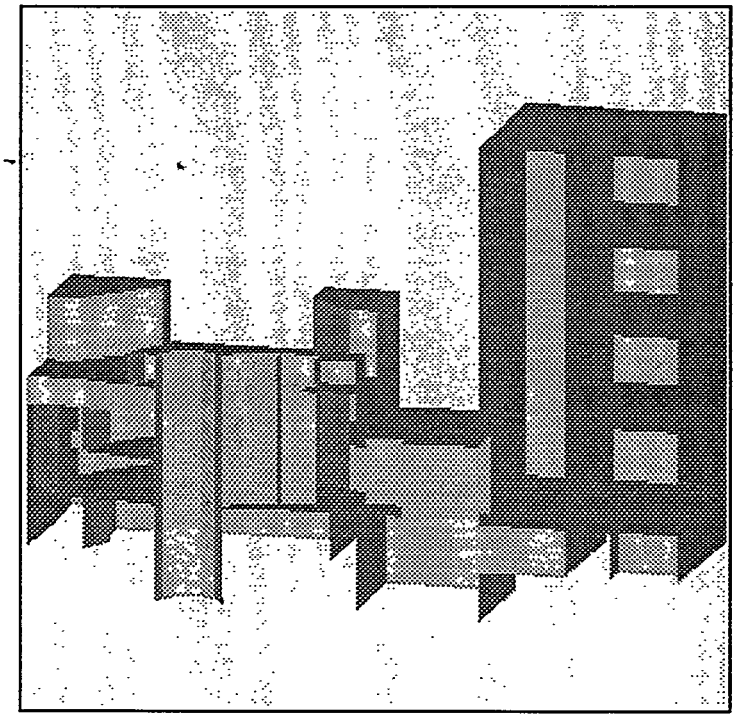

FIG. 6. INSIDE VIEW OF THE REACTOR BUILDING (LEFT) AND BUBBLER TOWER (RIGHT)

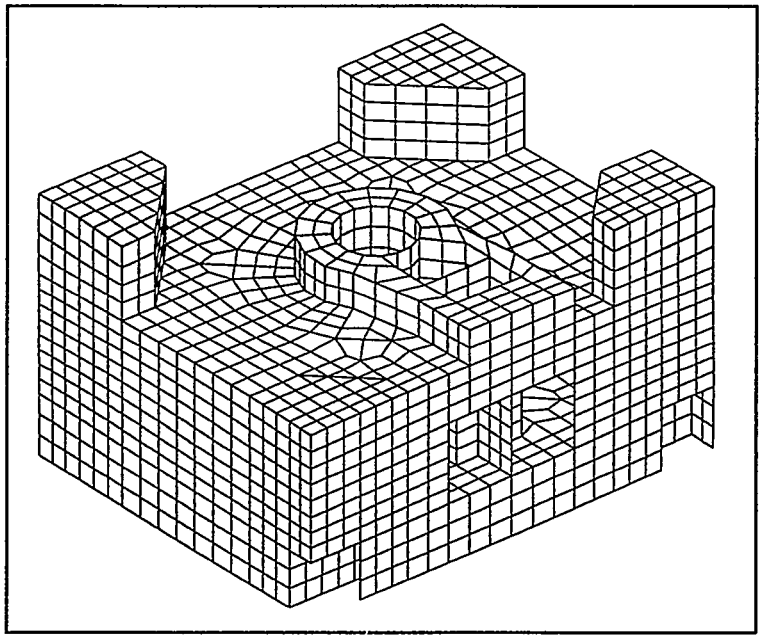

FIG. 7. FINITE ELEMENT MESH OF REACTOR BUILDING

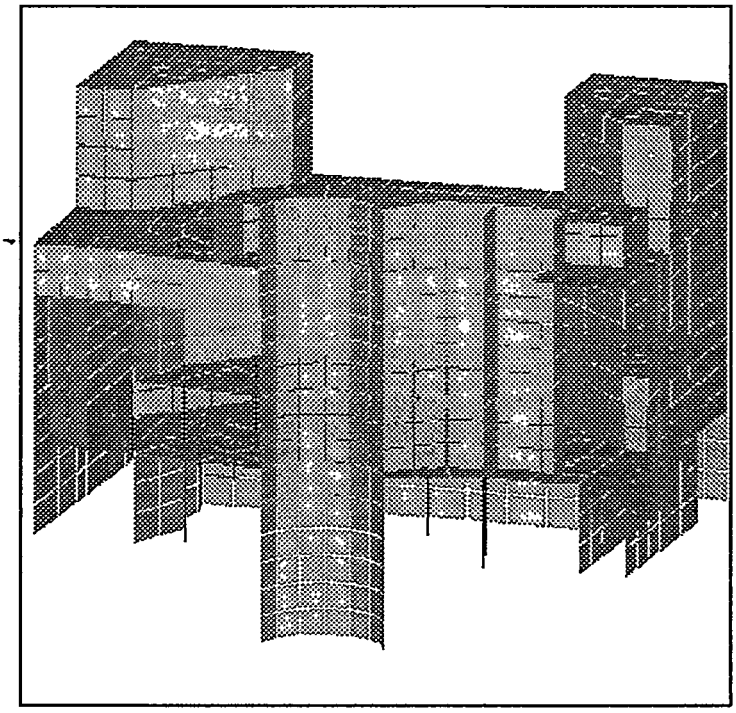

FIG. 8. CUT AWAY VIEW OF FINITE ELEMENT MESH OF REACTOR BUILDING

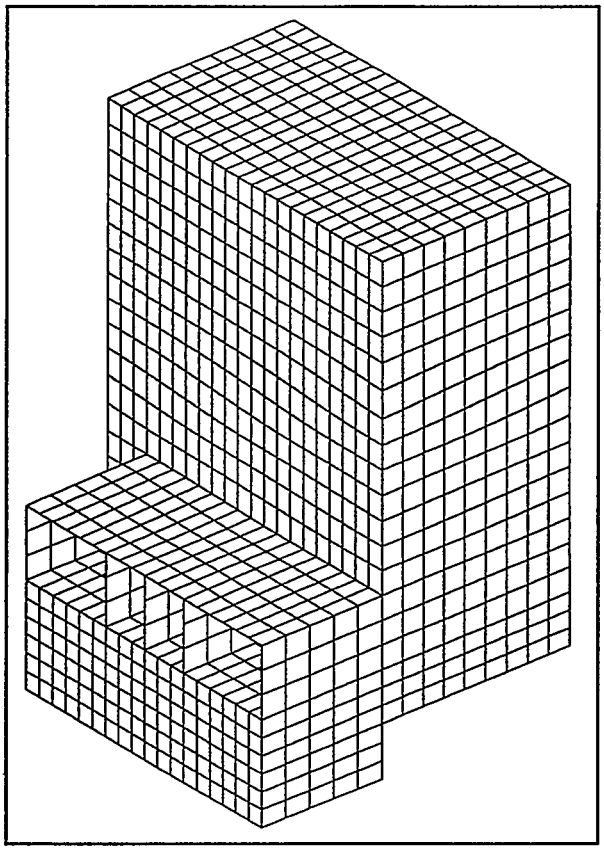

FIG. 9. FINITE ELEMENT MESH OF BUBBLER TOWER

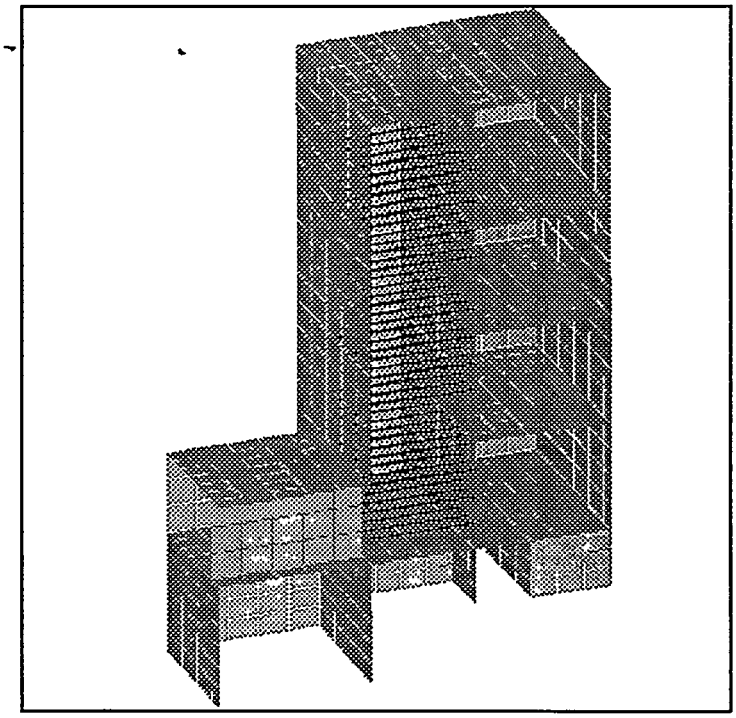

FIG. 10. CUT AWAY VIEW OF FINITE ELEMENT MESH OF BUBBLER TOWER

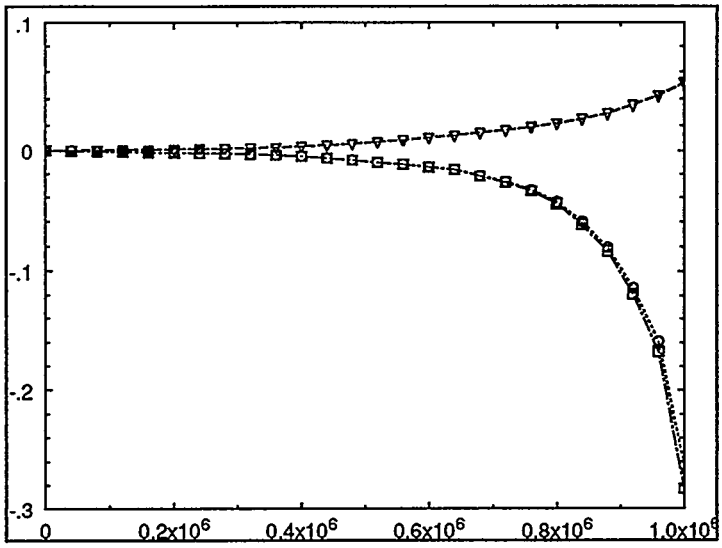

FIG. 11. MAXIMUM DISPLACEMENT OF REACTOR BUILDING VS. INTERNAL PRESSURE

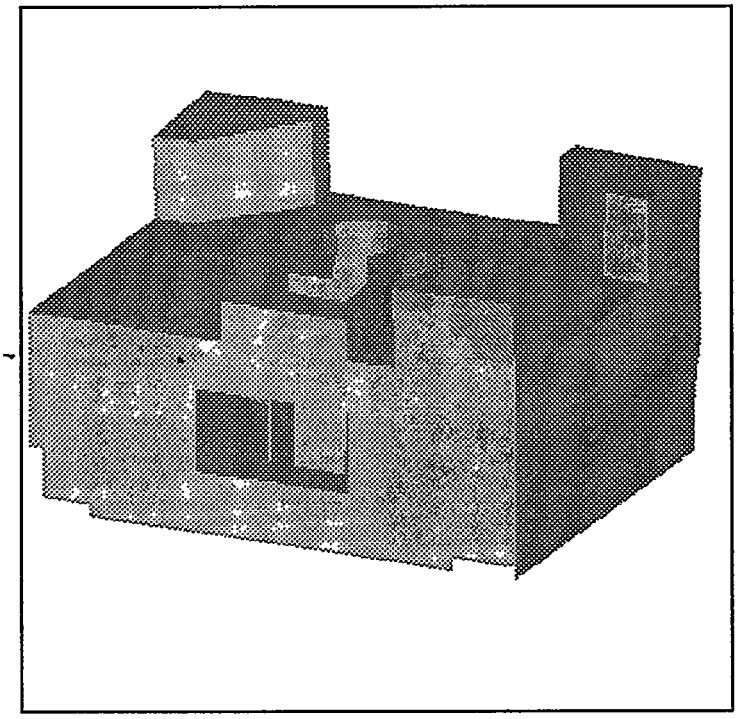

FIG. 12. DEFORMED SHAPE OF REACTOR BUILDING AT 1.0 MPA; MAGNIFIED BY 10

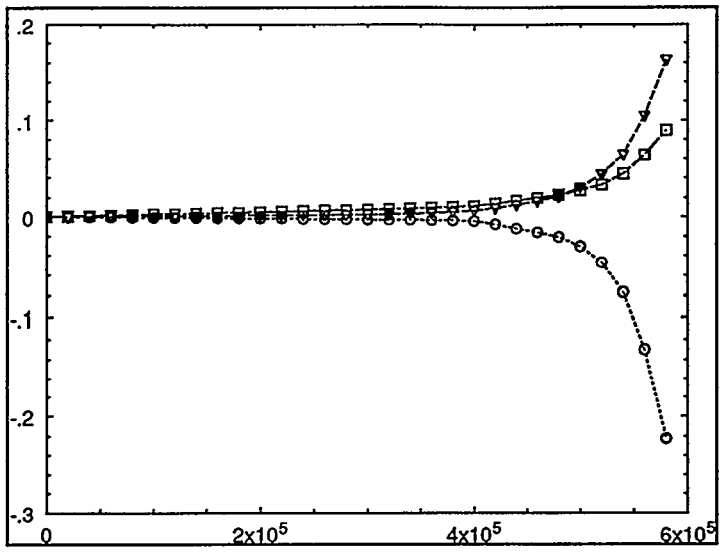

FIG. 13. MAXIMUM DISPLACEMENT OF BUBBLER TOWER VS. INTERNAL PRESSURE

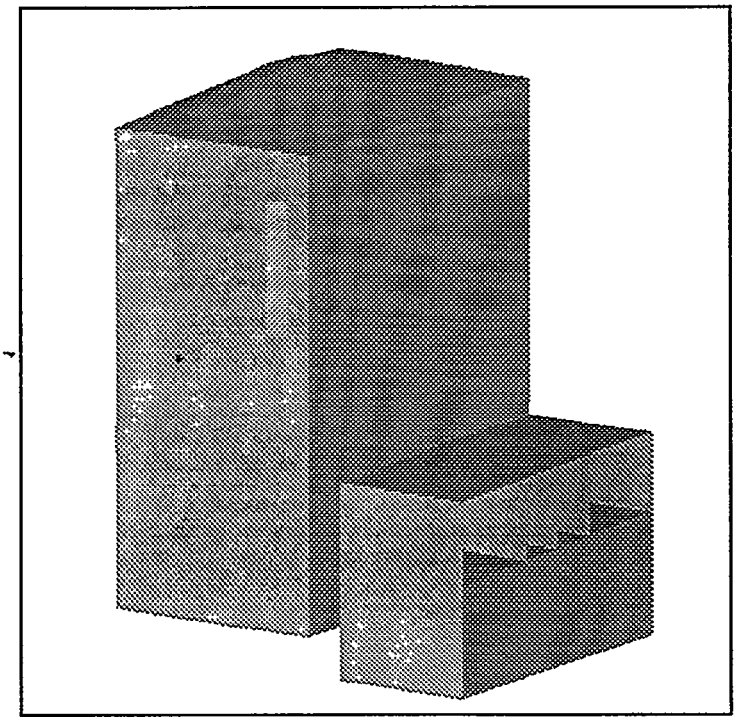

FIG. 14. DEFORMED SHAPE OF BUBBLER TOWER AT 0.58 MPA; MAGNIFIED BY 10

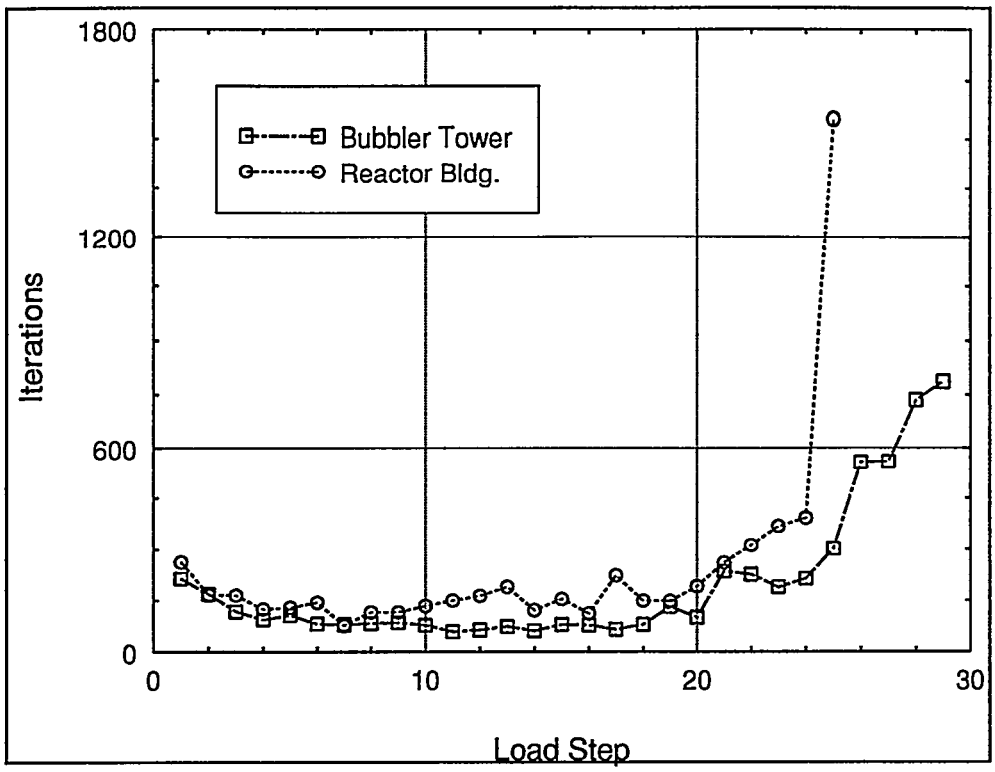

FIG. 15. DYNAMIC RELAXATION ITERATIONS VS. LOAD STEP FOR BOTH FINITE ELEMENT MODELS

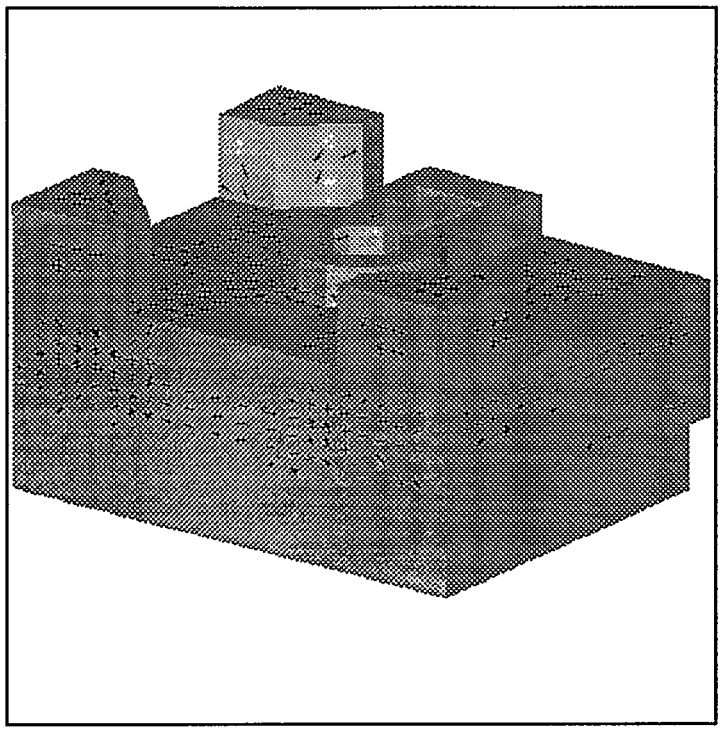

FIG. 16a. CRACKING PATTERN FOR OUTSIDE SURFACE OF REACTOR BUILDING AT 0.54 MPA; EAST (LEFT)AND NORTH (RIGHT) WALLS

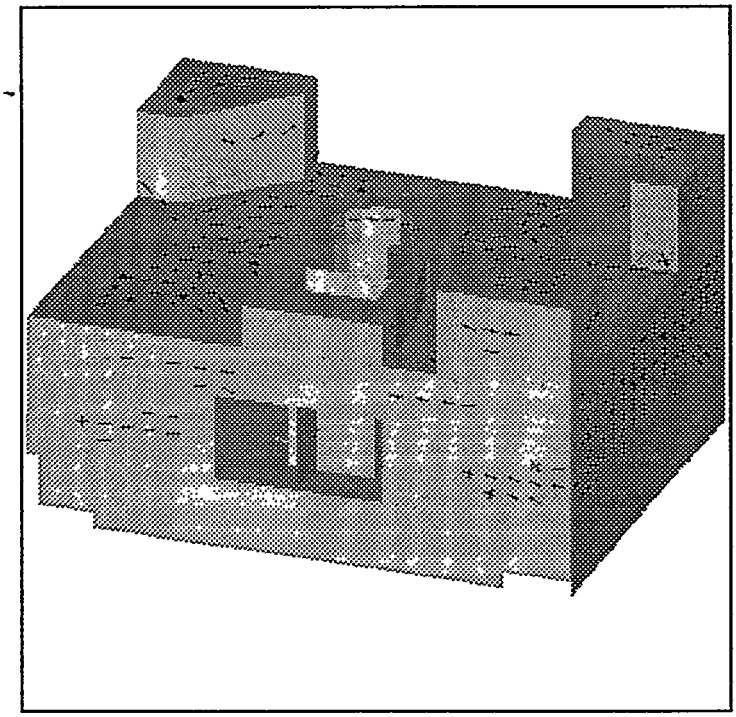

FIG. 16b. CRACKING PATTERN FOR OUTSIDE SURFACE OF REACTOR BUILDING AT 0.54 MPA; WEST (LEFT) AND SOUTH (RIGHT) WALLS

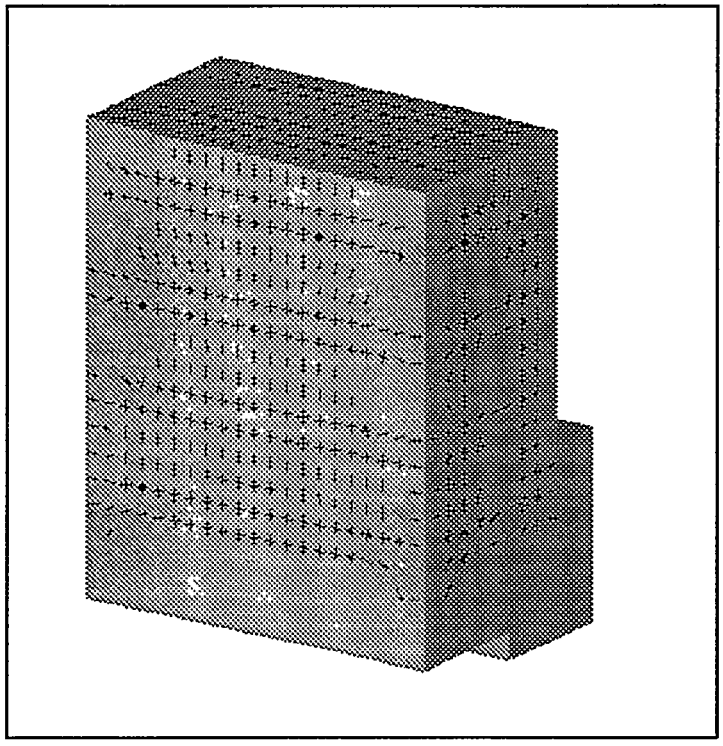

FIG. 17a. CRACKING PATTERN FOR OUTSIDE SURFACE OF BUBBLER TOWER AT 0.60 MPA; WEST (LEFT) AND SOUTH (RIGHT) WALLS

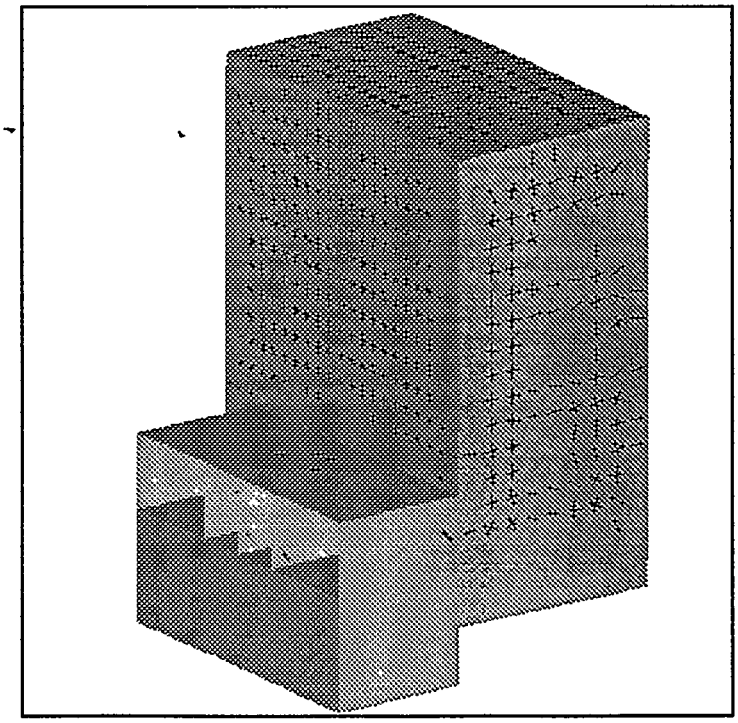

FIG. 17b. CRACKING PATTERN FOR OUTSIDE SURFACE OF BUBBLER TOWER AT 0.60 MPA; EAST (LEFT) AND NORTH (RIGHT) WALLS

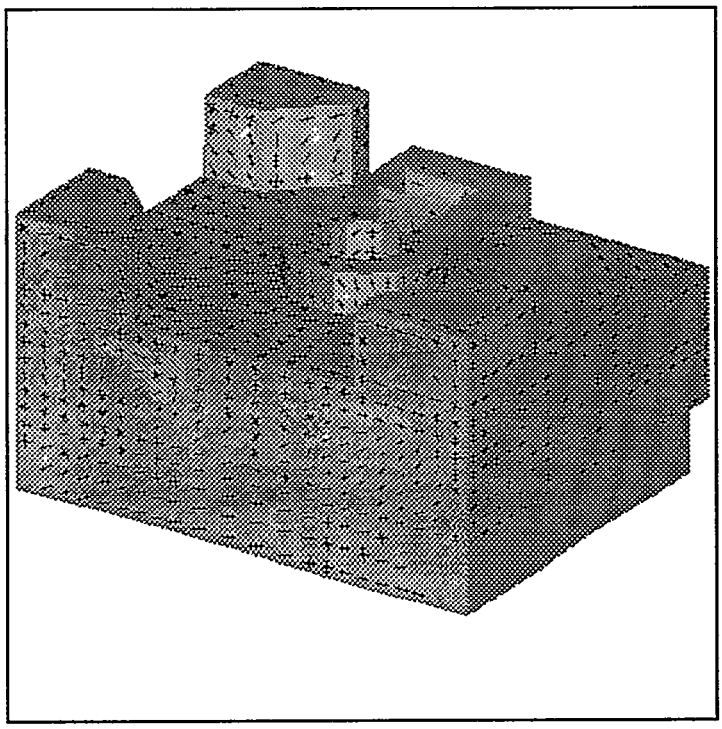

FIG. 18a. CRACKING PATTERN FOR REACTOR BUILDING AT 1.0 MPA OF EAST (LEFT) AND NORTH (RIGHT) WALLS; INSIDE SURFACE

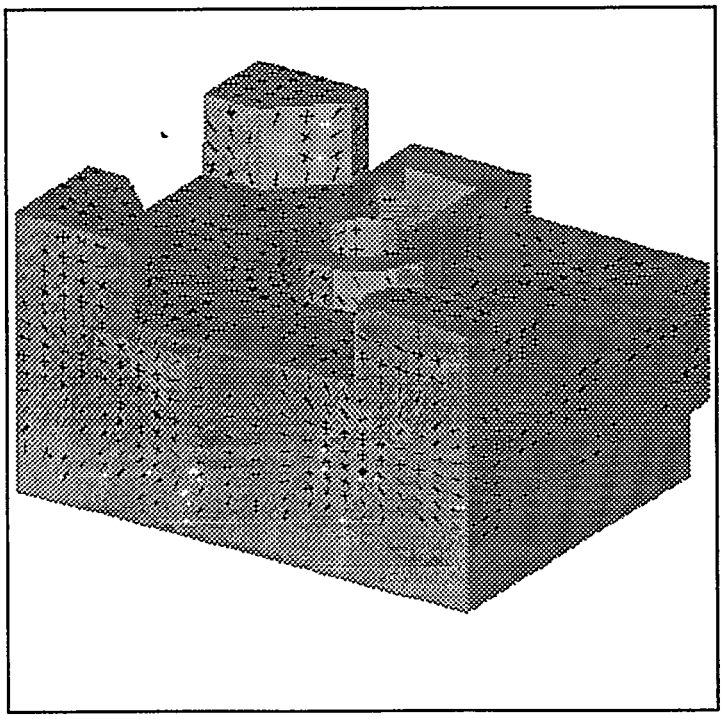

FIG. 18b. CRACKING PATTERN FOR REACTOR BUILDING AT 1.0 MPA OF EAST (LEFT) AND NORTH (RIGHT) WALLS; OUTSIDE SURFACE

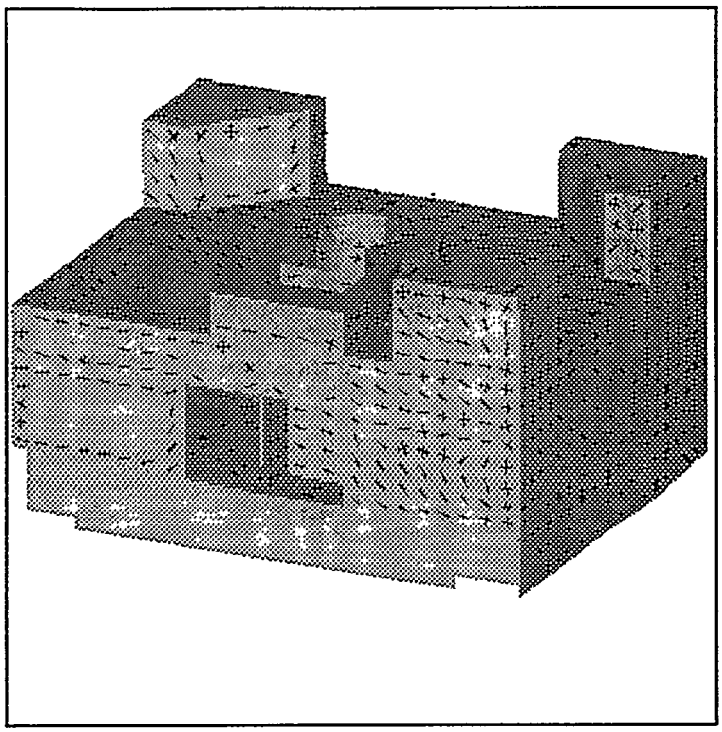

FIG. 19a. CRACKING PATTERN FOR REACTOR BUILDING AT 1.0 MPA OF WEST (LEFT) AND SOUTH (RIGHT) WALLS; INSIDE SURFACE

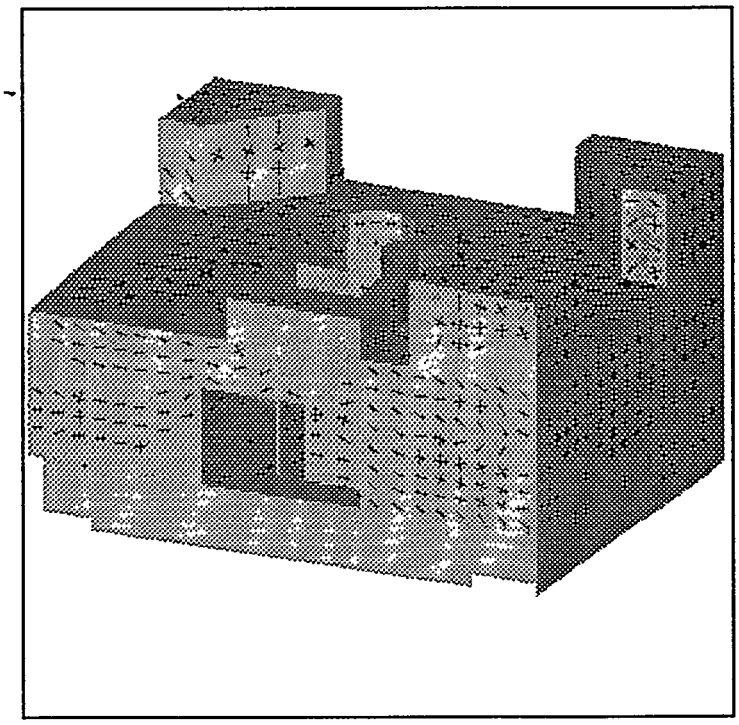

FIG. 19b. CRACKING PATTERN FOR REACTOR BUILDING AT 1.0 MPA OF WEST (LEFT) AND SOUTH (RIGHT) WALLS; OUTSIDE SURFACE

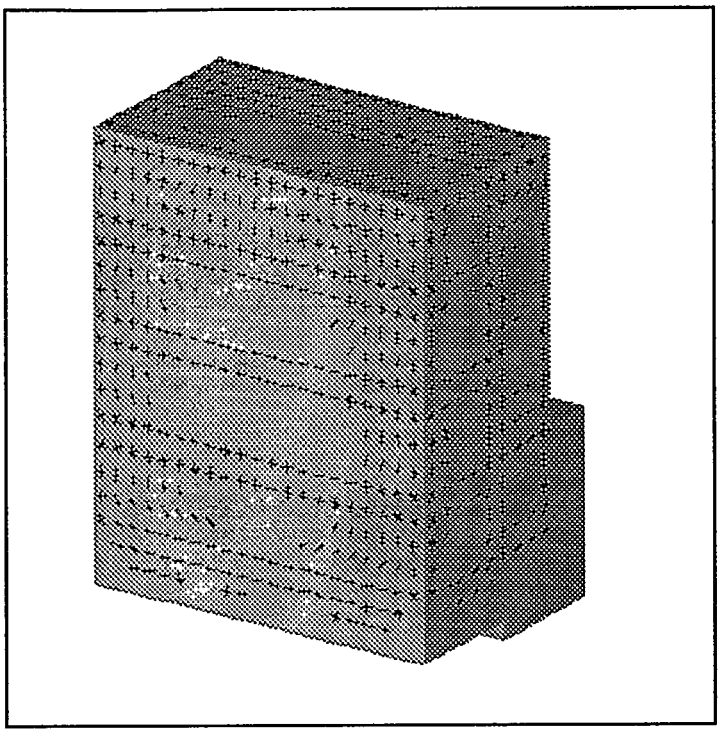

FIG. 20a. CRACKING PATTERN FOR BUBBLER TOWER AT 0.58 MPA OF WEST (LEFT) AND SOUTH (RIGHT) WALLS; INSIDE SURFACE

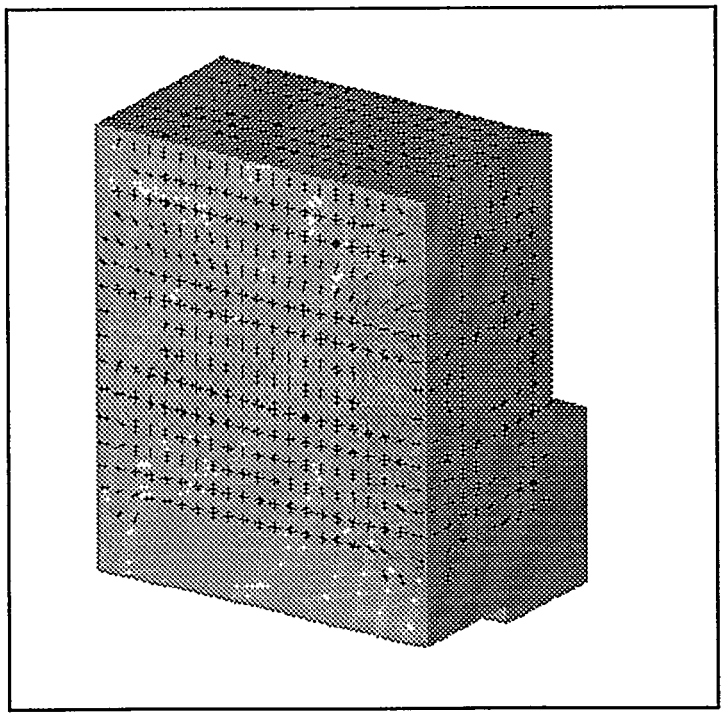

FIG. 20b. CRACKING PATTERN FOR BUBBLER TOWER AT 0.58 MPA OF WEST (LEFT) AND SOUTH (RIGHT) WALLS; OUTSIDE SURFACE

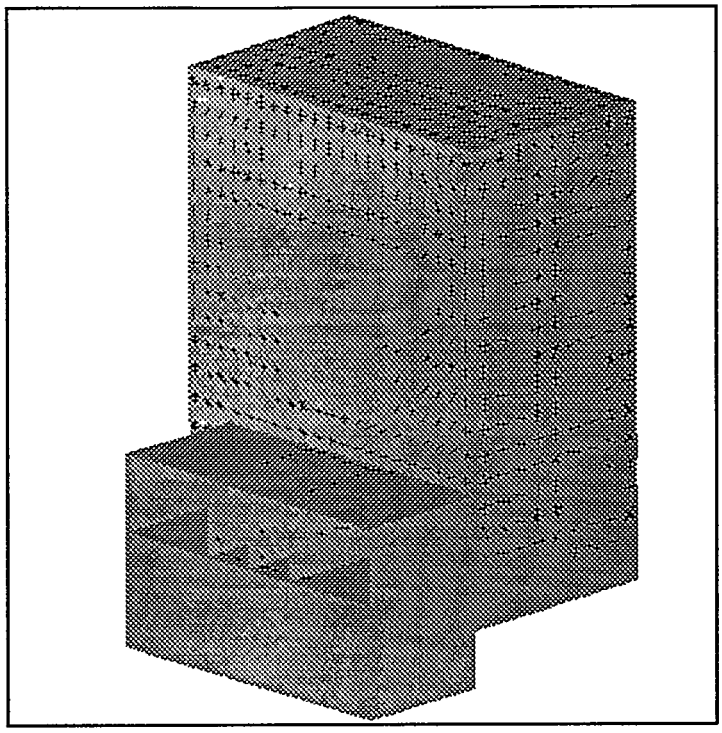

FIG. 21a. CRACKING PATTERN FOR BUBBLER TOWER AT 0.58 MPA OF EAST (LEFT) AND NORTH (RIGHT) WALLS; INSIDE SURFACE

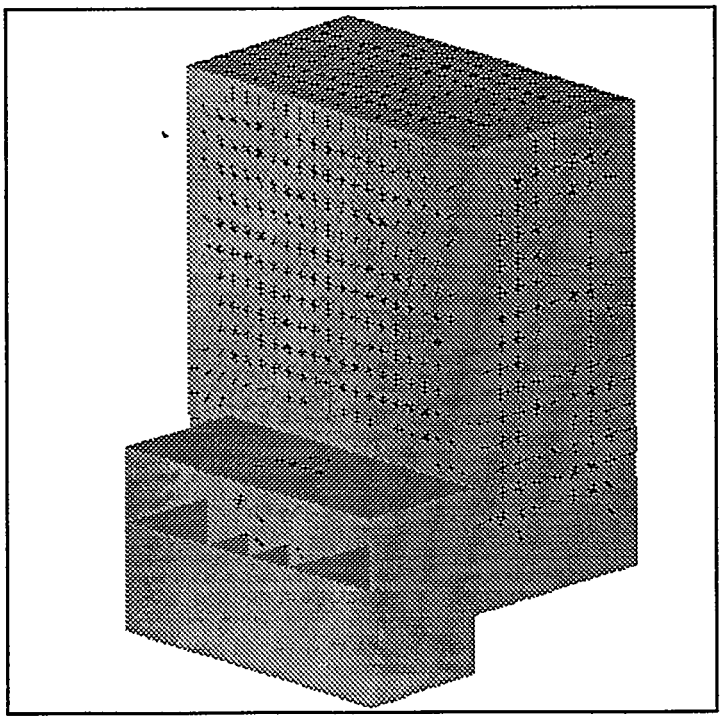

FIG. 21b. CRACKING PATTERN FOR BUBBLER TOWER AT 0.58 MPA OF EAST (LEFT) AND NORTH (RIGHT) WALLS; OUTSIDE SURFACE